Image Cover Sheet

CLASSIFICATION	SYSTEM NUMBER
UNCLASSIFIED	511896

TITLE

Transmission Electron Microscopy of Laser Surface Melted Nickel Aluminum Bronze Alloys

System Number:

Patron Number:

Requester:

Notes: Paper #22 contained in Parent sysnum #511874

DSIS Use only:

Deliver to: CL

Transmission Electron Microscopy of Laser Surface Melted Nickel Aluminum Bronze Alloys

by J.C. Bennett[1] and C.V. Hyatt[2]

[1]Department of Physics, Acadia University, Wolfville, Nova Scotia, B0P 1X0
[2]Defence Research Establishment Atlantic, Dockyard Laboratory, P.O. Box 99000 Stn Forces, Halifax, Nova Scotia B3K 5X5

ABSTRACT

Nickel aluminum bronze alloys are susceptible to a number of surface sensitive degradation processes during service in marine environments. Surface engineering using laser melting and cladding techniques has demonstrated a potential to substantially enhance performance, however little data is currently available on the microstructures developed in these materials. In this study, the microstructure of a series of experimental nickel aluminum bronze alloys containing from 8 to 12 wt. % Al, 3.8 to 6.5 wt. % Ni, 3.8 to 6.5 wt. % Fe, ~ 1 wt. % Mn plus additions of Ti and Zr was examined using transmission electron microscopy. The distributions, morphologies and crystal structures of the phases/precipitates present were found to vary significantly with the nominal alloy composition. For quaternary alloys having in excess of 11.30 wt. % Al, the microstructure mainly consists of martensitic β' plates containing a high density of small, Fe-rich precipitates of the κ_{IV} type. For lower Al contents, the proportion of proeutectoid α along the prior β grain boundaries and Widmanstätten α within these grains is observed to increase when the Ni/Fe ratio is below unity while β' appears to be stabilized for Ni/Fe ratios greater than unity. Additions of Ti and Zr lead to the formation of intermetallic precipitate phases and also appear to influence the relative stability of the α and β' phases. The observed microstructures will be discussed in terms of the phase relationships developed during cooling from the melt.

Transmission Electron Microscopy of Laser Surface Melted Nickel Aluminum Bronze Alloys

J.C. Bennett
Department of Physics, Acadia University

C.V. Hyatt
Defence Research Establishment Atlantic

Outline

- Nickel Aluminum Bronze Phase Diagram
- Objectives
- Experimental Technique: TEM
- Materials
- TEM Observations
- Conclusions and Future Work

Nickel Aluminum Bronze Phase Diagram

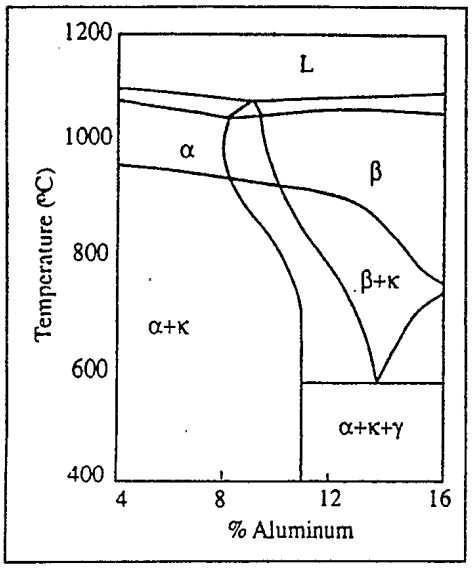

Typically contain 9 -12 wt. % Al

Al < ~11 wt. %:
α solid solution (fcc)
κ phases: κ_I, κ_{II}, κ_{IV} (Fe_3Al prototype)
κ_{III} (NiAl prototype)

Al > 11 wt. %:
β solid solution (bcc)
γ: martensite → 2H

Rapid cooling:
"retained β": martensite → 9R or 18R

Vertical Section of Cu-Al- 5 wt. % Ni -5 wt. % Fe Equilibrium Phase Diagram

Background

- Laser cladding techniques developed by DREA have demonstrated a potential to improve surface properties.
- Interest in developing an optimum consumable alloy with less sensitivity to heat input, better ductility, etc.

Problem:

- Melt cooling rates are inherently high in laser surface treatments → the microstructure forms far from equilibrium.
- Little data is currently available on microstructural development in NiAl bronzes under these conditions.

Objectives:

- Determine phase distributions, structural defects, etc., produced in several alloys under varying heat inputs.
- Improve understanding of the effects of the various microstructural features on the surface properties.

Transmission Electron Microscopy

Techniques:

- Selected area electron diffraction
- Convergent beam electron diffraction
  - *crystallographic information from matrix and precipitate phases as small as 10 nm²*
- Diffraction contrast electron microscopy
- High resolution electron microscopy
  - *direct imaging of crystal structures and lattice defects (stacking faults, twins, dislocations) with near atomic resolution.*
- Energy dispersive x-ray microanalysis
  - *semi-quantitative elemental analysis from small volumes ~ 100 nm³*

Materials

1.) NiAl Bronze Laser Cladding

Base casting: Cu-8.6 % Al-4.4 % Ni-4 % Fe-1.1 % Mn
Welding wire: Cu-9.0 % Al-4.6 % Ni-3.9 % Fe-1.2 % Mn
Laser heat input: 1.2 kJ/cm

2.) Gleeble Simulated NiAl Bronze Weldments

Base alloy: Cu-9.2 % Al-4.7 % Ni-3.4 % Fe-0.8 % Mn
Thermal Cycle: i) Peak temp 1040 °C → water quench (750 °C/s)
ii) Peak temp 1040 °C → air quench (188 °C/s)

3.) Experimental NiAl Surface Melted Alloys

Alloy	Cu	Ni	Fe	Mn	Al	Cr	Ti	Zr	Ni/Fe
1	76.45	5.06	6.20	0.35	9.70		2.24		0.82
2	79.60	3.80	5.50	1.00	10.10				0.69
4	81.20	3.80	3.90	1.00	10.10				0.97
5	78.60	6.50	4.60	1.10	9.20				1.41
7	77.95	4.00	5.80	0.95	11.30				0.69
9	77.30	4.60	4.60	1.00	12.50				1.00
12	79.30	4.10	4.30	1.00	11.30				0.95
23	78.95	4.70	5.00	1.00	8.90	0.60	0.44	0.41	0.94
24	80.60	3.70	4.40	0.91	7.80	1.12	0.79	0.68	0.84
27	78.63	4.90	5.3	1.10	9.30	0.31	0.23	0.23	0.92
CDA958		4.5	4.0	1.2	9.0				> 1

Experimental Details

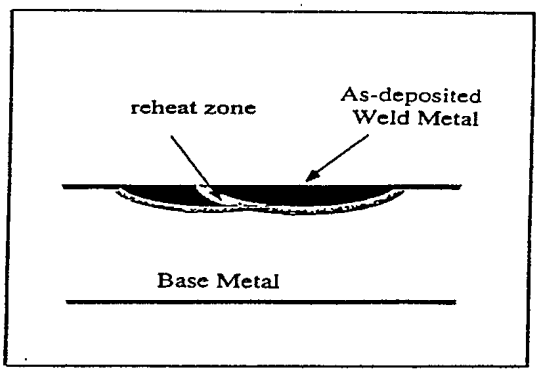

- Specimens prepared in plan view.
- Procedure: (i) weldment sectioned parallel to the clad surface
  (ii) mechanically back-thinned to 0.1 mm
  (iii) 3 mm diameter disks punched for TEM
  (iv) disks were ground to ~ 100 μm
  (v) electropolished (33% HNO3 in methanol, -30 °C, 10 V)
- Examined at 200 kV in Philips CM20 and 100 kV in Philips EM301

NiAl Bronze Laser Cladding

Optical micrograph

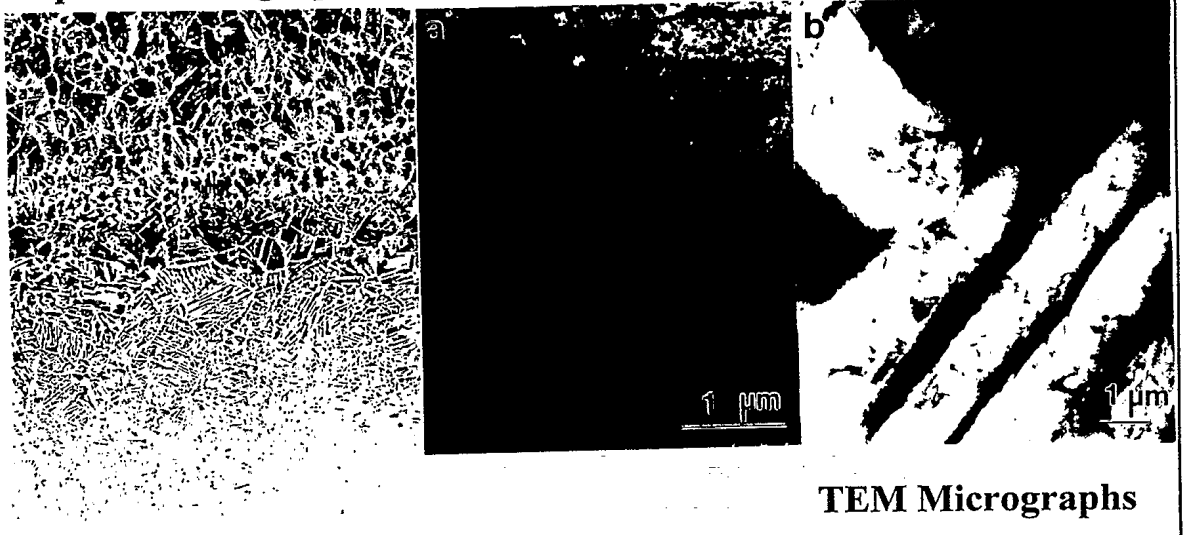

TEM Micrographs

(a) as-deposited: (i) light plates (basket-weave), (ii) dark irregular plates
(iii) high density of small (~20 nm) precipitates

(b) reheat zone: (i) light phase (plates and equiaxed), (ii) dark plates
(iii) high density of precipitates in the dark phase

Laser Clad *as-deposited* Region: Light Plates

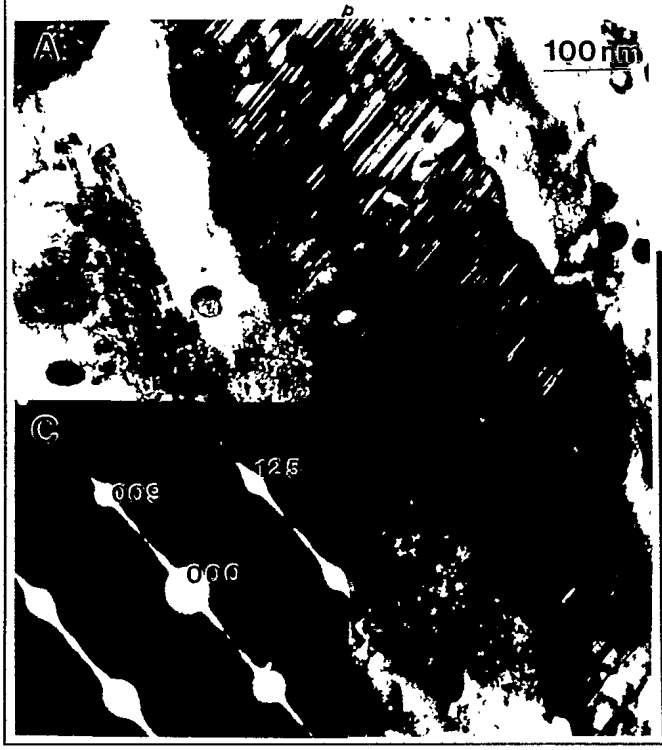

A: Bright Field Image
B: HREM image
C: $[2\bar{1}0]_{ortho}$ z.a. SAED pattern

CDA 95800
Cu-9 wt.% Al-4.5 wt.% Ni-4.0 wt. % Fe-1.2 wt.% Mn, Heat Input 3000 J/cm

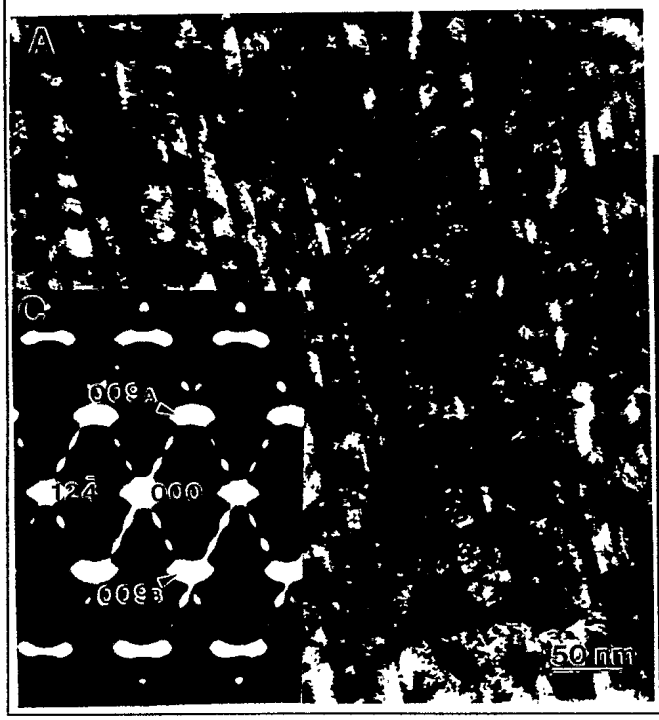

A: Bright Field Image
B: HREM image
C: $[2\bar{1}0]_{ortho}$ z.a. SAED pattern

Laser Clad NiAl Bronze Phase Distribution

as-deposited region

Light plates:
- *9R structure*: long-range ordering of close-packed $\{111\}_{fcc}$ layers
- average stacking order ABCBCACAB is disturbed by many random faults
- orthorhombic unit cell (a = 0.449 nm, b = 0.519 nm, c = 1.91 nm)

Dark Plates:
- *9R structure*: narrow (~ 20 nm) twin-related domains $(101)_{tp}$
- semi-coherent due to random faulting

The 9R structure occurs for martensites in related systems (e.g. Cu-Al).

Small precipitates (~ 20 nm diameter):
- numerous in both light and dark plates
- microdiffraction patterns consistent with Fe_3Al type structure (κ_{IV} precipitates)

reheat region

Light plates and grain boundaries: α phase (fcc, a = 0.365 nm)

Dark plates: similar to as-deposited region

Small precipitates: κ_{IV} type in martensite, few found in α

Gleeble Weld Simulations: Water quenched

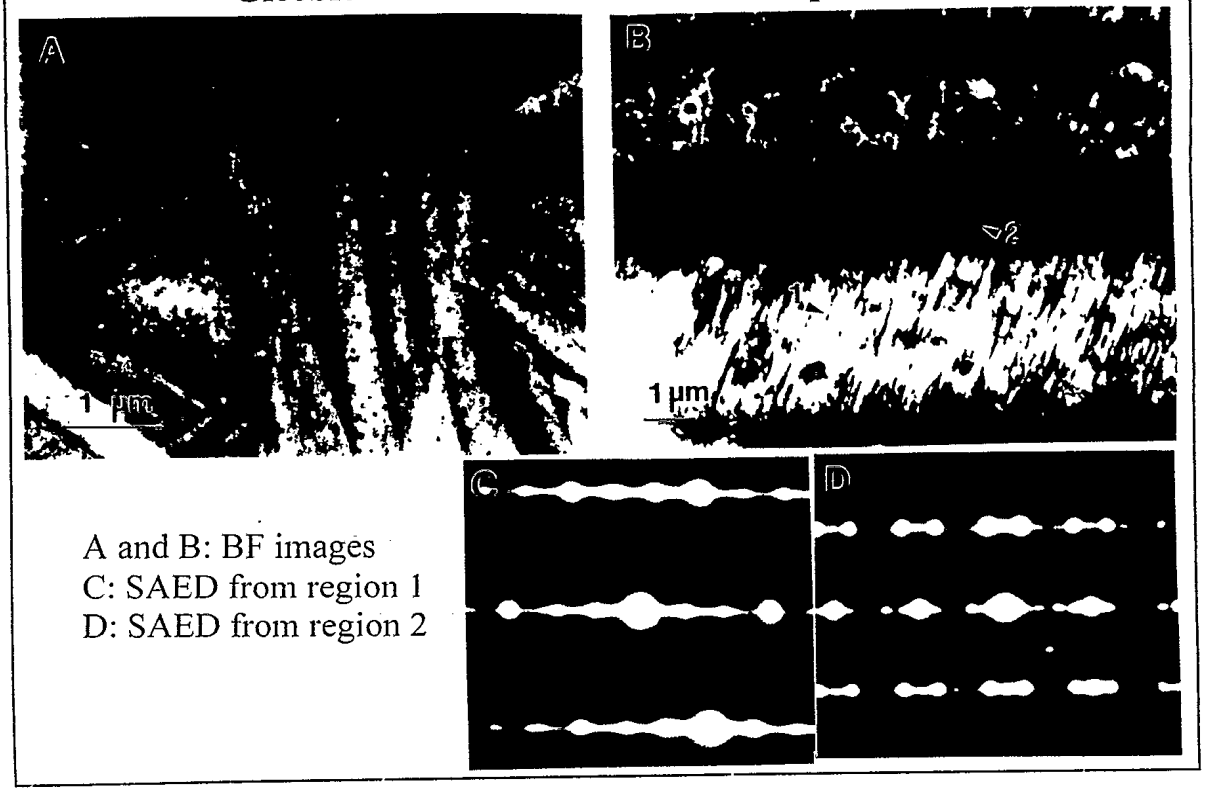

A and B: BF images
C: SAED from region 1
D: SAED from region 2

Gleeble Weld Simulations: air quenched

A: Bright field image of eutectoid region ($\alpha + \kappa_{III}$)

B: SAED pattern from elongated precipitate (NiAl, κ_{III} type)

Similar eutectoid regions are common in the reheat zone and less frequent in the as-deposited material.

CDA 95800
Cu-9 wt.% Al-4.5 wt.% Ni-4.0 wt. % Fe-1.2 wt.% Mn, Heat Input 25 J/cm

A: Low magnification BF image (M: martensite, a: α phase)

B: BF image of a typical grain interior showing *mottle* contrast

CDA 95800
Cu-9 wt.% Al-4.5 wt.% Ni-4.0 wt. % Fe-1.2 wt.% Mn, Heat Input 25 J/cm

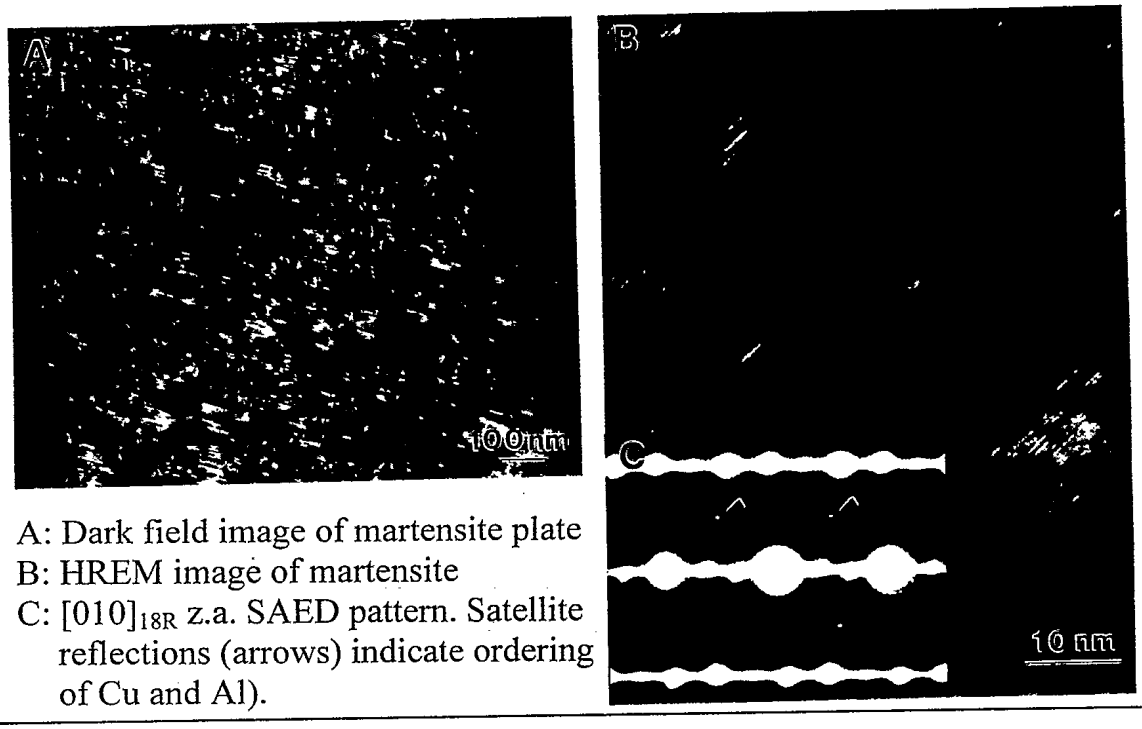

A: Dark field image of martensite plate
B: HREM image of martensite
C: $[010]_{18R}$ z.a. SAED pattern. Satellite reflections (arrows) indicate ordering of Cu and Al).

Cu-9.2 wt.% Al-6.5 wt.% Ni-4.6 wt. % Fe-1.1 wt.% Mn, Heat Input 800 J/cm

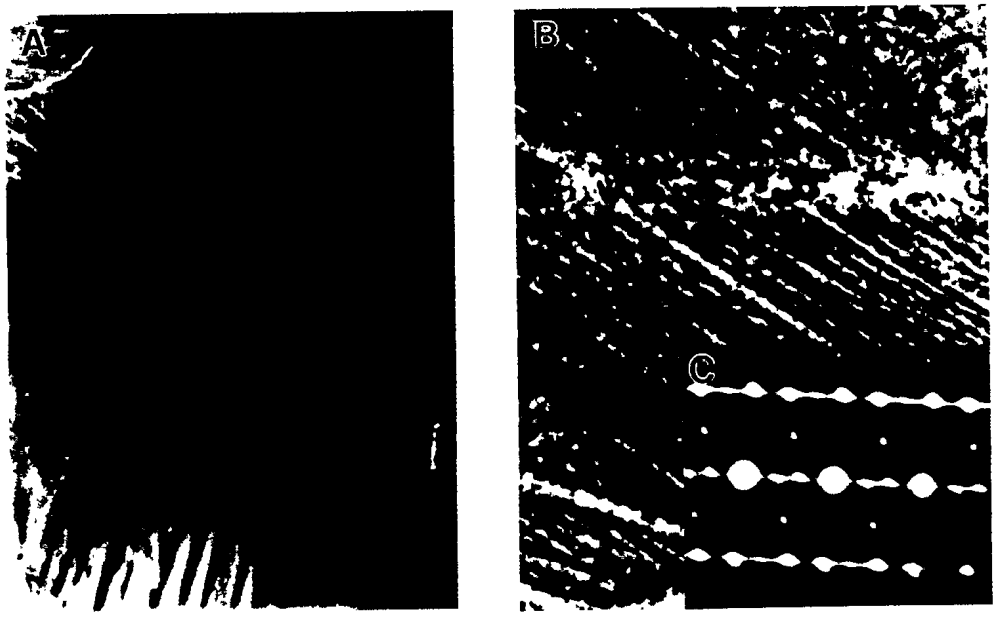

A: Low magnification image showing martensite in grain interiors.
B: BF image of martensite plate
C: $[010]_{18R}$ z.a. SAED pattern from martensite.

Cu-11.3 wt.% Al-4.0 wt.% Ni-5.8 wt. % Fe-0.9 wt.% Mn,
Heat Input 3000 J/cm

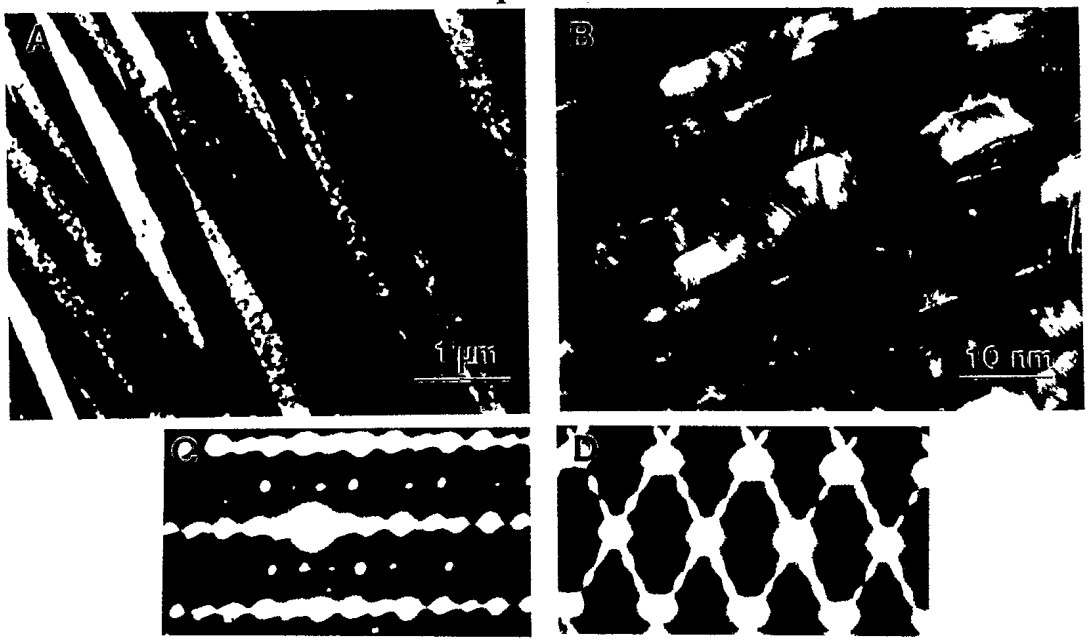

A: Low magnification image showing martensite in grain interiors.
B: [010] z.a. HREM image of martensite plate
C, D: $[010]_{18R}$ and [210] z.a. SAED patterns from martensite.

Cu-12.5 wt.% Al-4.6 wt.% Ni-4.6 wt. % Fe-1.0 wt.% Mn
Heat Input 3000 J/cm

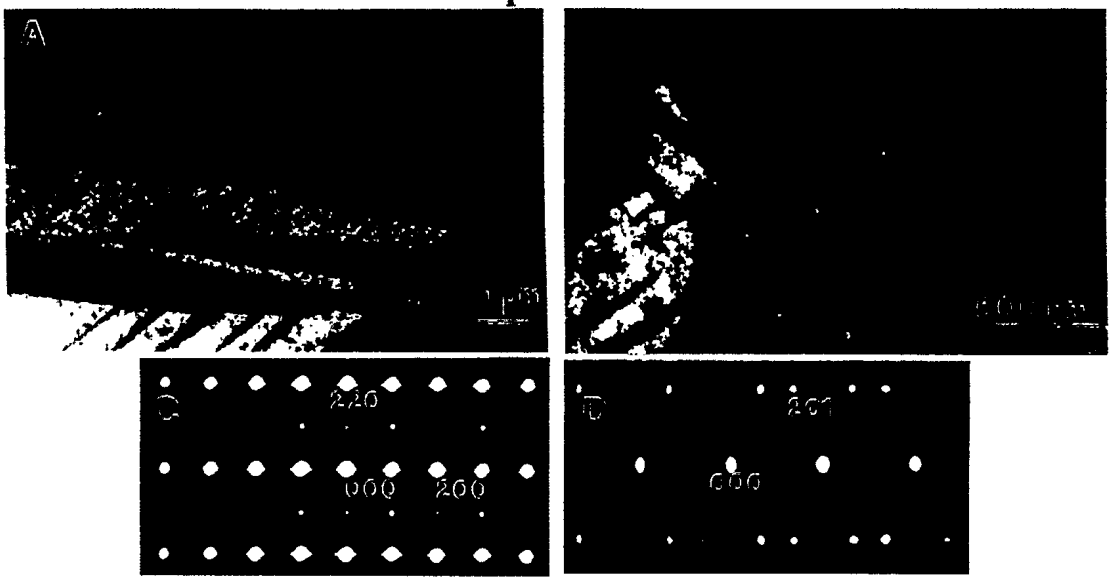

A: Low magnification image.
B: Bright field image of γ' martensite
C: $[010]_{18R}$ z.a. (equivalent to $[1\bar{1}00]_{2H}$) SAED pattern from γ' martensite.
D: $[2\bar{1}4]_{18R}$ z.a SAED twinned on the (121) plane.

Cr-Ti-Zr bearing Nickel Aluminum Bronze

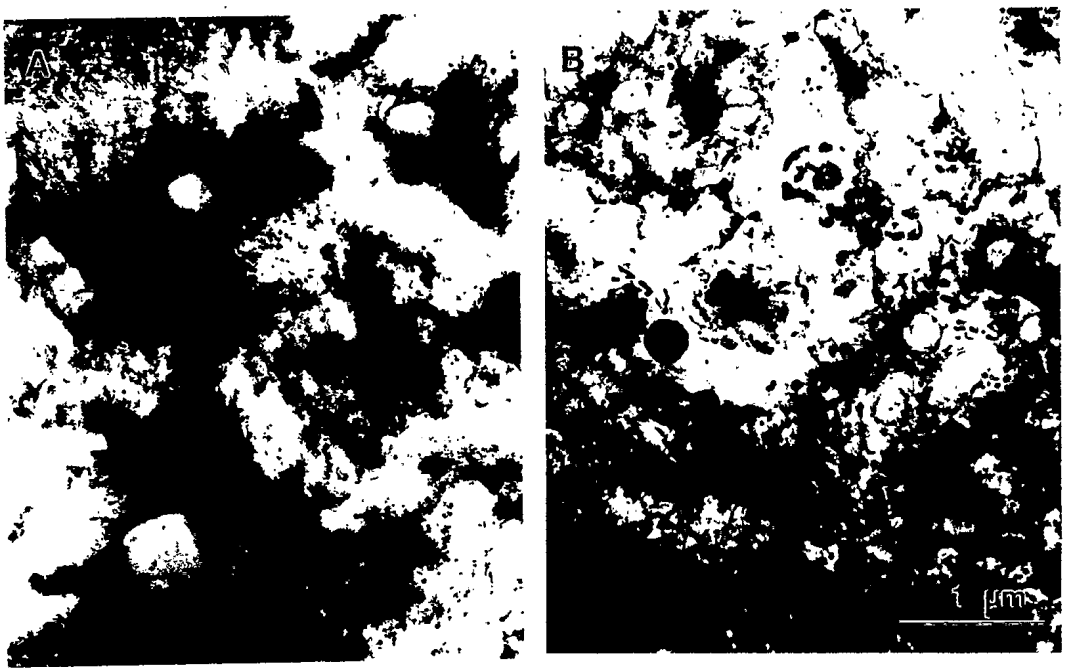

BF images: Cu:Al:Ni:Fe:Mn:Cr:Ti:Zr
A: 78.9:8.9:4.7:5.0:1.0:0.6:0.44:0.41; B: 80.6:7.8:3.7:4.4:0.9:1.1:0.8:0.7

Cr-Ti-Zr bearing Nickel Aluminum Bronze

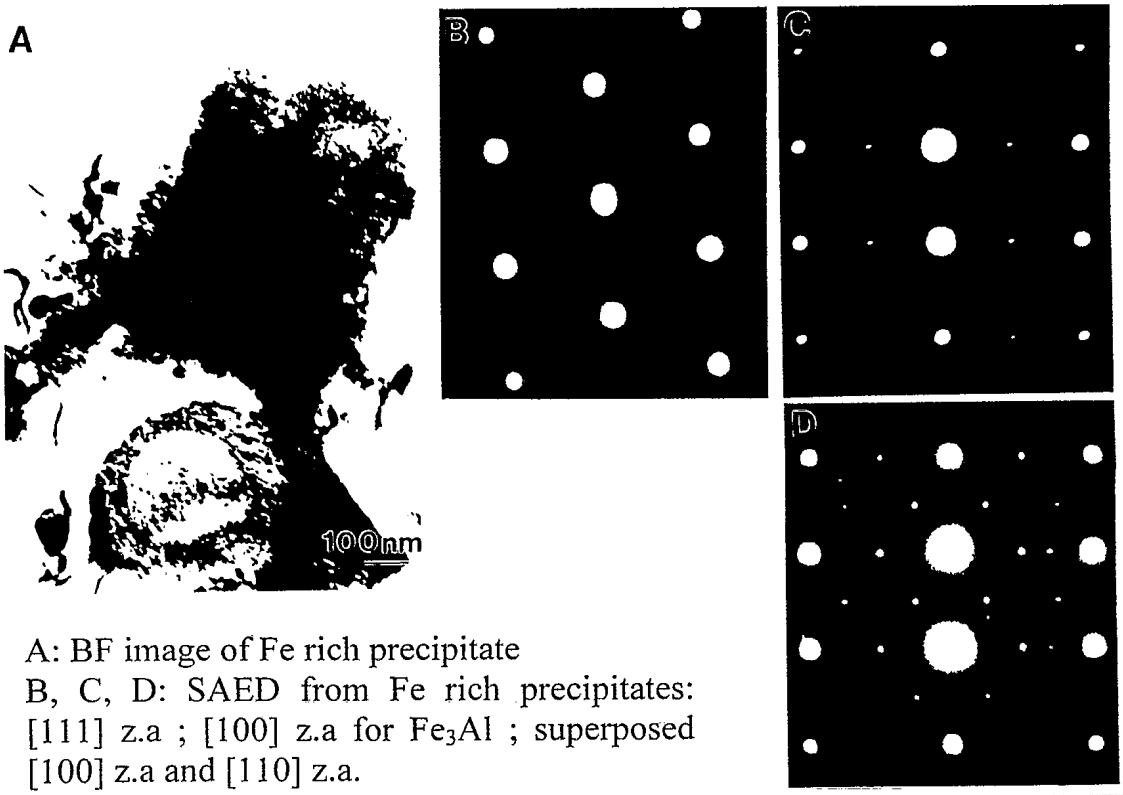

A: BF image of Fe rich precipitate
B, C, D: SAED from Fe rich precipitates: [111] z.a ; [100] z.a for Fe_3Al ; superposed [100] z.a and [110] z.a.

Conclusions

- TEM has been used to characterize the phase distribution developed in nickel aluminum bronze during laser cladding.
  - phases include α phase (allotriomorphic and Widmanstatten), two morphologies (i.e. plate sizes) with 9R structure, small Fe rich κ_{IV} precipitates, and (α + Ni rich κ_{III}) eutectoid.
- Simulated welds that were water quenched from 1040 °C developed a microstructure within the grains similar to that observed in the as-deposit region of the laser clads.
  - the large domain α plates adopt the 9R structure exclusively
- Simulated welds that were air cooled from 1040 °C developed a microstructure somewhat different than that observed in the reheat zone of the laser clads.
  - proportion of eutectoid appears to be increased
- Laser surface melting CDA 95800 with heat input 25 J/cm produced α at the grain boundaries and 9R martensite within the grains.
  - contain a very high density of small (< 10 nm) coherent precipitates

Conclusions

- A high density of Fe-rich precipitates was observed in all martensite phases.
- Ni content of 6.5 wt. % produced some ordering of the β' martensite (to 18R). Martensite predominates in the interior of the grains.
- Ordered β' martensite (18R) was observed for all samples studied with Al concentration exceeding 11 wt. % independent of Ni/Fe ratio. Again predominately martensite (both morphologies) within grains
- For the sample containing 12.5 wt. % Al, β' (majority phase) and γ' (minority phase) martensites were observed.
- Cr, Ti and Zr additions resulted in major microstructural changes. The α phase was found to be inter-dispered, irregular martensite plates. Large Fe rich κ_{II}/κ_{IV} type and irregular Zr rich precipitates were found to be numerous.